Available online at www.sciencedirect.com

ScienceDirect

journal homepage: www.elsevier.com/locate/he

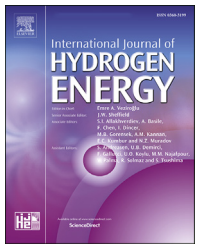

Microstructural investigation of the effect of electrospraying parameters on LSCF films

Can Sındıraç [a,b], Sedat Akkurt [a,*]

[a] Izmir Institute of Technology, Department of Mechanical Engineering, Izmir, Turkey
[b] ASPILSAN Energy Industry and Trade Inc, Istanbul, Turkey

HIGHLIGHTS

- ESD is a new technique used for coating thin cathode layers on GDC electrolyte.
- The effect of electrospraying parameters on LSCF cathode layer microstructure is studied.
- A new type of solvent couple (mixture of ethylene glycol & 2-butoxyethanol) is employed.
- Cathode layer with desirable stoichiometric ratio of LSCF was achieved.
- Encouraging results were obtained in EIS measurements (i.e., 0.82 Ω cm^2).

ARTICLE INFO

Article history:
Received 28 October 2019
Received in revised form
20 February 2020
Accepted 26 February 2020
Available online 21 March 2020

Keywords:
ESD
SOFC
Electrospray deposition
Cathode
Polymeric precursor solution
Electrolyte

ABSTRACT

Intermediate temperature solid oxide fuel cells (IT-SOFC) require an effectively functioning cathode layer whose performance depends largely on their microstructures. Improved electrochemical performance of the cathode layer can be possible by tailoring the microstructure to ensure that both the oxygen reduction reaction (ORR) occurs fast along the triple-phase boundaries (TPB) and the diffusion pathway is short enough for fast ion diffusion through the cathode layer. Electro spray deposition (ESD) method is a low-cost deposition method which allows the optimization of microstructure by changing the spraying parameters. In this study, gadolinium doped ceria (GDC) electrolyte layer is deposited with $La_{1-x}Sr_xCo_{1-y}Fe_yO_{3-\delta}$ (LSCF) derived from polymeric precursor salts, symmetrically. As a solvent couple, 2-butoxyethanol and ethylene glycol are used instead of the conventional solvent couples frequently employed in the literature. The use of the new type of solvents in the precursor solution leads to promising results on modifying the microstructure of the deposited layer. The effect of electrospraying parameters on the cell performance was also studied. Promising results were obtained as measured by impedance spectroscopy when this new solvent couple was employed.

Introduction

Solid oxide fuel cells (SOFCs) are clean energy sources which provide clean electricity by converting chemical energy into electrical energy without burning [1,2]. Despite this critical advantage, it is still not yet fully commercialized because of the excessive cost of components used at high operating temperatures (i.e., 800–1000 °C) [3]. Reduction of the operating

* Corresponding author.
E-mail address: sedatakkurt@iyte.edu.tr (S. Akkurt).
https://doi.org/10.1016/j.ijhydene.2020.02.194

temperature to 500–700 °C has been proposed to save on the cost of materials and components resulting in a new type of SOFCs called Intermediate-Temperature (IT-SOFC) [4]. Besides, start-up and shut-down processes are significantly shortened, which is crucial for portable device applications [5]. Although there are several advantages derived from lowered operating temperature, there is a drawback in electrochemical performance, resulting mainly from compromised electrochemical properties of the traditional electrolyte (e.g., Yttria Stabilized Zirconia-YSZ) and cathode (e.g., Lathanium Strontium Manganese-LSM) layers [6]. Great effort has been devoted to find some strategies to compensate for this performance drop [7]. One of the first proposed strategies was to replace the traditional materials with new candidate materials that do not suffer from loss of electrochemical performance in the low temperature range (i.e., 500–700 °C). Mixed ion-electron conductor (MIEC) perovskite oxides have been selected as potential cathodes (i.e., $La_{1-x}Sr_xCo_{1-y}Fe_yO_{3-\delta}$-LSCF) instead of their traditional counterpart (i.e., LSM) which only exhibit electronic conductivity with negligible ionic conductivity [8–10]. MIECs can also enlarge the triple phase boundaries (TPB) of catalytic oxygen reduction reaction (ORR) area [8–12]. New electrolyte materials were also a necessity due to sluggish ionic conductivity of YSZ in the new low temperature range. Gadolinium doped ceria (GDC) was proposed as an alternative electrolyte material of YSZ since GDC is chemically and physically compatible with LSCF [13,14].

Since performance of SOFC is mostly limited by the performance of the cathode layer, selection of both the cathode material and its microstructure is vital [15]. It is known that the formation process of the cathode layers directly effects the resulting microstructure and performance of the cell [15,16]. It is not uncommon to obtain different electrochemical properties after different formation techniques are applied to the same material [15,17,18]. There are different techniques (chemical, physical and other) to form cathode layers of SOFCs [13,17,19]. Chemical methods include i) Chemical Vapor Deposition (CVD), which is based on adsorption of gaseous species onto the substrate [20,21], and ii) formation of thin films via precursor solution by thermal treatment onto the substrate like atomic layer deposition (ALD) [19]. Physical methods are classified as i) Physical Vapor Deposition (PVD) which involves different types of sputtering methods like radio-frequency and magnetron sputtering [22], ii) laser deposition methods such as Pulsed Laser Deposition (PLD) which leads to the formation of desired film on a substrate via vaporization by laser beams [23–25]. Finally, other methods are screen printing, tape casting which helps deposit a ceramic slurry on a ceramic substrate through open mesh and/or doctor blade, respectively [26,27]. Besides, spin and dip coating techniques are quite common techniques [28]. These techniques are mostly based on metal-organic decomposition for the formation of cathode films via decomposition of a chemical solution containing precursor salts upon heating. These precursor solutions may be used in dipping, spinning, or brush painting [19]. All these techniques have advantages and disadvantages. One of the most important drawbacks in chemical and physical methods is the necessity to use expensive types of equipment. Although, other ceramic processing methods are relatively cheaper; ceramic methods require mostly extensive labor work and careful work to control ceramic slurries [17,29]. To overcome this problem, Electrospray Deposition (also known as electrostatic deposition or electrostatic atomization of liquids or simply ESD) method is proposed as a low-cost, fast, and facile method [15,30–32]. Even though electro-spraying was invented earlier in the last century and has been used in painting industry due to its high deposition efficiency [33–36], it has also been employed for the formation of thin/thick films from aerosols which are used in a wide variety of fields [17,37–39]. Electrostatic atomization of liquids has been used in many different fields of industry for many years. However, these techniques are now used for the formation of functional metal oxide layers in SOFCs (i.e., $LaCoO_3$, LSCF, YSZ, GDC, etc.), solar cell perovskites, solid-state lithium-ion batteries (i.e., $LiCoO_2$, $LiMn_2O_4$, Li_3PO_4, SnO_2–MnO_2) and chemical sensors [17,19,30–43].

There are several advantages of these techniques as i) simple and low-cost setup without any vacuum system ii) a wide variety of low-cost precursor solutions, iii) relatively large film growth rate, iv) ambient atmosphere operation, v) control of the morphology of deposited layers, vi) control of the stoichiometry in precursor solutions and deposited layers [17,40,42,44]. The deposited layers may either be dense or porous compared to other expensive control techniques such as sol-gel, CVD, RF sputtering, injection-LPCVD [40,45,46], and vii) applied in various fields [17].

ESD involves the use of a precursor solution which is blown through a nozzle by the help of a syringe pump, that turns into an aerosol under high voltage maintained between the nozzle and the target. On its way to the heated target (electrolyte pellet), this aerosol rapidly evaporates and strikes the surface at high velocity [46]. Because of the nano-dimensions, they quickly decompose and form the mixed oxide layer at the surface of the electrolyte. A porous cathode layer forms in a "coral" structure, which is highly desirable for efficient ORR [30]. There are several parameters that affect the quality of spraying (i.e., flow rate, exposure time, substrate temperature, the value of high voltage, the distance between needle and substrate). When the deposition parameters are controlled well, the desired microstructure can be formed on the cathode layer which may bring about improvements in the electrochemical performance [15]. In this study, some of these parameters were investigated to find out an optimum microstructure for best SOFC performance. In the literature, the precursor solution used for ESD is mostly prepared by using ethanol and butyl carbitol solvent couple [15,17,18,30–32,37,40]. This solvent acts as a carrier agent to supply the necessary ions to form the mixed oxide cathode layer in the precalculated stoichiometric proportions. Princivalle [47] indicated that this solvent couple had a greater effect on surface tension and the density of a precursor solution [48,49]. In this study, a different solution is tested for the first time in the literature. Composed of 2-butoxyethanol and ethylene glycol, this new solution is known to exhibit better capillary action properties into the pores due to inherent wetting properties. These solvents are ethylene glycol and 2-butoxyethanol which are the same solvents used for preparing the infiltration solution as can be seen in previous studies of the authors [50–52]. Further, the effect of the use of this

new solvent is discussed by looking into how it affects the resulting cathode layer coating micro-structure. In the recent years, some significant and promising results were achieved via methods which used polymeric precursor method with this solvent couple [50,52]. Therefore, it is well worth to investigate this solvent couple, whether it can be successfully used in ESD. To the best of our knowledge, these solvents have not been comparatively studied before.

Microstructures of prepared samples were investigated with Scanning Electron Microscope (SEM). Energy Dispersive X-ray Spectroscopy (EDX) analysis was used to find out the elemental distribution in the coated cathode layer. This study is focused on experimental control of the morphology of the deposition layer by varying the deposition parameters. Selected samples were investigated by Electrochemical Impedance Spectroscopy (EIS) method to characterize the electrochemical performance of symmetrical cells.

Experimental set-up and procedure

10 mol % gadolinium-doped ceria (denoted as GDC, $Ce_{0.9}Gd_{0.1}O_3$, PRAXAIR >99.9%) was used for preparing the electrolyte substrate discs. The powder with a specific surface area of 6.5 m^2/g was pressed in cylindrical stainless steel die (15 mm diameter) by uniaxial pressing (Carver Hydraulic Press, Wabash, IN, USA) using 180 MPa of pressure. These pellets were used as electrolyte layers to be coated by ESD and tested in a symmetrical cell configuration. In order to obtain gas-tight electrolytes, the pellets needed to be almost completely dense, so they were fired in an electrically heated laboratory kiln (Nabertherm LHT 02/17, Germany) at 1400 °C for 8 h soaking time at a heating/cooling rate of 3 °C/min.

ESD process requires the use of a precursor solution to be deposited on the electrolyte to constitute the cathode layer via pyrolysis of the same solution. Hence, LSCF polymeric precursor must contain stoichiometric amounts of the constituent cations. Lanthanum (III) nitrate hexahydrate (ALFA-AESAR >99.99%), strontium chloride hexahydrate (ALFA-AESAR >99%), cobalt (II) nitrate hexahydrate (ALFA-AESAR >97.7% min), iron (III) nitrate nonahydrate (ALFA-AESAR >99.99%) salts were mixed in deionized water and ethylene glycol at a molar ratio that will eventually produce the $La_{0.6}Sr_{0.4}Co_{0.8}Fe_{0.2}O_3$ stoichiometry. The total concentration of the cation ratio to the solution was fixed to 0.02 M. Then, it was stirred at 80 °C until polymerization took place, and water evaporation process was finished. Finally, the solution was diluted with 2-butoxyethanol to reduce the surface tension of the polymeric precursor solution. Hence, the wetting properties of resultant solutions were enhanced. Further details of the process are given elsewhere [50–52]. These solvent couples were chosen based on the experiences of the authors in previous studies [50–52].

A vertical electrospray deposition (ESD) set-up was designed in house by the authors (Fig. 1). The precursor solution was pumped by a syringe pump at a controlled flow rate (New Era NE-1000). The solution was passed through a metallic needle (i.e., hypodermic needle). Tip of hypodermic needle is available in an angle-cut shape, so by the help of a Dremel Tool needle tip was cut to obtain a blunt tip to enhance spraying conditions. The outer diameter of needle was 0.50 mm. A high voltage power supply (PlusElectronic 3000 High Voltage Supply, Turkey) was used to ensure that high voltage is applied between the needle (also called as nozzle or capillary) and the target metal plate. The solution was atomized into an aerosol owing to the high applied voltage between the tip of the needle and the substrate. Vertical design was necessary to avoid gravitational forces which might have complicated the deposition quality. The round electrolyte pellet specimen (substrate) was seated on a 10 mm diameter hole in the center of the aluminum plate. The working distance between the needle and the substrate were varied between 23 and 28 mm. A positive high voltage was chosen in the range of 7–15 kV by a DC high voltage power supply. The tip of the needle was monitored with a camera to observe the spraying modes. Substrate temperature was maintained between 300 and 400 °C by an electrical resistance heater which was connected to a programmable controller (Eurotherm Controller, 2216e). Heating was necessary to ensure that the solvents inside the polymeric precursor have completely evaporated and remaining cations deposited as films on pore surfaces. As a final factor, deposition time was varied between 30 and 90 min. In order to prepare a symmetrical cell, both sides of electrolytes were coated with the same conditions. After the deposition process was finished, samples were annealed at 700 °C for 2 in an electrically heated laboratory kiln (Nabertherm LHT 02/17, Germany) for the crystallization process in the ambient atmosphere. Heating and cooling rates were also chosen as 3 °C/min.

In order to find out the ability of the ESD method, both microstructural and compositional analysis were performed by Scanning Electron Microscopy (SEM, Philips XL 30S FEG) utilizing secondary electron (SE) imaging on cross-sections of the samples. Energy dispersive x-ray spectroscopy (EDX) was used for elemental analysis. Crystal structures were examined by x-ray diffraction (XRD, Panalytical X-Pert Pro). Cu Kα radiation was selected as the x-ray source.

In order to investigate the electrochemical performances of coated samples, an in-house Ag paste was brush-painted onto both sides of electrodes. Polarization resistance behaviours of cathode samples were measured by using Methrohm (Autolab) potentiostat in the ambient atmosphere in the range of 500–700 °C. The electrochemical impedance spectroscopy (EIS) was performed in a typical frequency range of 1 MHz-0.01 Hz with a 15 mV excitation amplitude. The measured data were fitted by using Autolab Nova 2.1 software.

Results and discussions

As this study was aimed at investigating the suitability of the use of polymeric precursor solutions in coating a cathode layer on a GDC substrate using ESD process, process parameters of ESD were important. If successfully coated, how the experimental conditions would effect the structure of the coated LSCF layers was the main research question in the present study. The present work is focussed on investigating the effects of solvent couple, prepared by ethylene glycol (EtGl) and 2-Butoxyethanol (2-BuEt) used in precursor solution on the microstructural and electrochemical properties of Electro

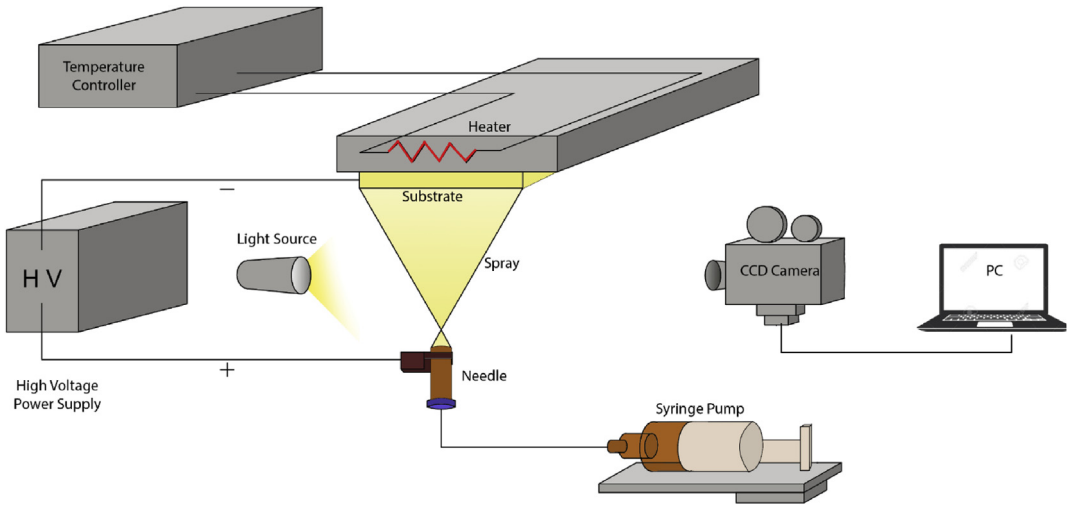

Fig. 1 – Sketch of the ESD set-up. Electrolyte specimen (substrate) sits upside down on the heated metal plate on which there is a 10 mm diameter hole. Potential difference between the heated metal plate and the needle draws the solution onto the target ceramic specimen.

Spray Deposited (ESD) LSCF cathode films on dense GDC electrolyte.

ESD process may be divided into three main parts: the atomization of polymeric precursor solution, transport of the charged droplets and formation of coating on substrate. Spraying mode directly effects these three parts. Adjusting the flow rates, applied voltage and distance between needle and substrate directly affects the capillary needle as cone-jet, multi-jet or dripping mode since the jet breaks up forming droplet clouds. The test results indicated that spraying strongly depended on the applied voltage. While voltages lower than 7 kV failed to form aerosol particles, increasing voltage rapidly brought about workable spraying modes (i.e., dripping or cone-jet mode). Owing to changes in voltage the spray modes varied from dripping mode (dripped drop by drop) to cone-jet mode and a further increase lead to transition of spraying mode from cone-jet to multi-jet which lead to segregated coating regions. Successful results were obtained in cone-jet mode. The continuous cone-jet (or multi-jet modes) was the most suitable mode for a homogenous fine well-dispersed coating (Fig. 2).

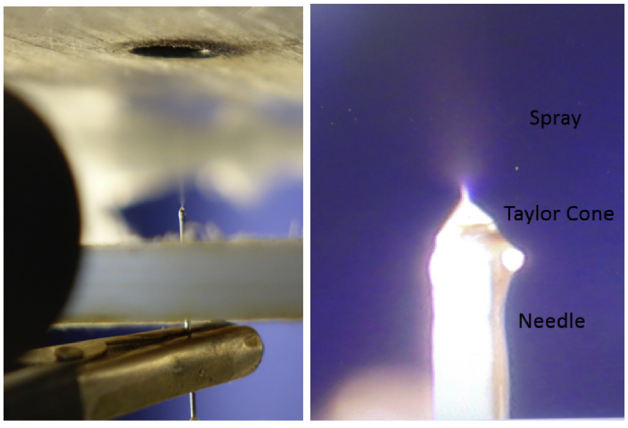

Fig. 2 – Formation of Taylor-Cone at the tip of needle. Notice the well-developed spray like a cloud.

Studied samples coated by EDS are listed in Table 1 with their deposition conditions like distance between tip of needle and substrate, flow rate of solution, sample temperature as controlled by the heating controller, and applied voltage. In each experiment, only one parameter was varied while all other factors were kept constant.

Fig. 3 depicts the surface morphology of LSCF layer which was deposited at a flow rate of 1 ml/h and 350 °C with 7 kV potential difference with working distance of 15 mm (Sample 1). Dripping mode of spraying meant that solution droplets reached the surface without much evaporation during flight while most of the evaporation took place on the surface hence leading to cracked, non-homogenous films (Fig. 3a). When, however, the applied voltage was increased to 11 kV, a more homogeneous coating was obtained in cone-jet mode (Sample 2). Other conditions (i.e., surface temperature, working distance and the flow rate) were, of course, kept the same (Fig. 3b). As shown in Fig. 3b, dripping mode leads to a segregated coating layer which is not acceptable. Sprayed droplets apparently travelled between the nozzle tip and the target without control which brought about cracks and hence non-

Table 1 – Summary of the Electro-Spray Deposition experimental conditions for investigated samples. Sample codes and the corresponding test conditions are listed.

Sample Code	Working Distance (mm)	Flow Rate (ml/h)	Sample Temp (°C)	Voltage (kV)
1	15	1	350	7
2	15	1	350	11
3	23	0.35	350	11
4	23	0.35	400	11
5	23	0.5	400	11
6	23	0.5	400	15
7	28	0.5	400	15

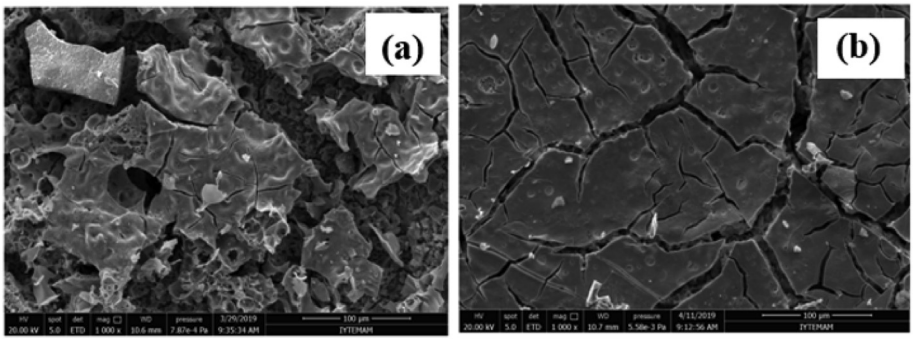

Fig. 3 – Surface morphologies of the LSCF layer on the GDC substrate (a) Sample 1 (deposited in dripping mode) and (b) Sample 2 (deposited in cone-jet mode) shows the surface.

homogenous surfaces. In order to assure consistent flow of charged droplets, a cone-jet mode is required which can be accomplished by increasing the applied voltage. Consequently, once the voltage was raised, a better-dispersed coating was obtained. From this point on at least 11 kV voltage was applied for other samples.

In order to obtain a more homogenous surface, the flow rate was reduced to 0.35 ml/h and working distance between the needle and the surface was increased to 23 mm to reduce the droplet size. To obtain a stable cone-jet mode, 11 kV was required (e.g., as shown in Fig. 4a for sample 3). After the best solution flow rate, deposition time and working distance were identified, the effect of substrate temperature was investigated. Uniformity of the cross-section of the deposited layers were investigated and it is seen that the distribution of particle sizes was not satisfactory. This semi-porous type coating was probably related with the substrate temperature which was 350 °C. This temperature was not enough to evaporate solvents in precursor solution during flight. Therefore, some reticulations and irregular networks were observed. Hence, the surface temperature was increased to 400 °C in order to ensure homogeneity with a thicker cathode layer (Sample 4-Fig. 4b). This temperature leads to increased evaporation rate, resulting in smaller droplets as mentioned by other studies [15,31,32,49].

A test involved the effect of flow rate as shown in Fig. 5. Coral structure with nano-porosity was observed in Sample 4 (Fig. 5a). This type of structure is useful in cathodes since it can offer more surface area for oxygen reduction. The way this structure develops may perhaps be explained by the successful access of droplets to the hot surface in such a way to cover the surface homogeneously, without large gaps. It is clearly seen that increasing the flow rate from 0.35 to 0.5 ml/h had little effect on degrading homogeneity and lead to repeated spraying and baking. This eventually leads to agglomeration (Sample 5-Fig. 5b). Increasing the flow rate at fixed potential difference, substrate temperature and working distance brought about enlarged size of droplets which indicated arrival of charged particles landing on the hot substrate surface since they were still partially wet. Eventually, that lead to some agglomeration as also reported by other groups [32,53,54].

As a final attempt, the distance between needle and substrate was further increased (Fig. 6) to find out higher porosity. However, on the surface, smaller particles are observed in Sample 7 (Fig. 6b) with large macro-cracks. Analysis of Samples 6 and 7 revealed the influence of working distance at the highest voltage. Further increasing of working distance (from 23 to 28 mm) with high voltage (15 kV) caused more distant pathway for flight. During the relatively long flight, solvent couple prematurely evaporated which lead to solidification of particles that tended to overlap during deposition. This phenomenon is also reported as preferential landing effect (in the literature) which occurred via electrostatic attraction between substrate surface and charged droplets [15]. Sample 6 had cracks between the agglomerated areas, but Sample 7 had higher macro-cracks between denser deposited areas. This was possibly due to evaporation occurring in an uneven

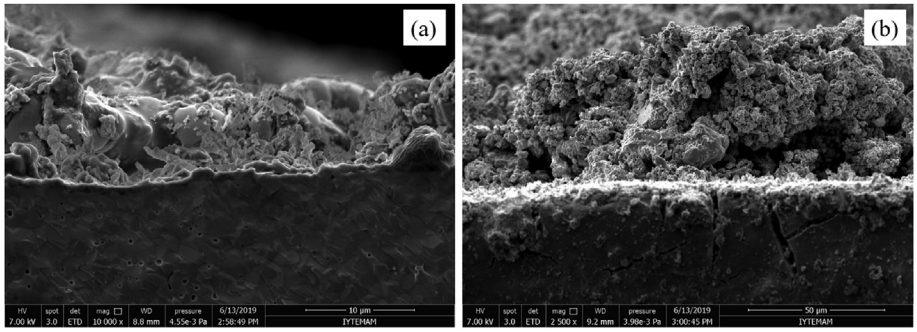

Fig. 4 – Cross sectional views of coated electrolyte. Top half of image shows the LSCF coating and GDC substrate. Surface morphologies of LSCF layers as deposited on GDC electrolyte. (a) Sample 3 and (b) sample 4.

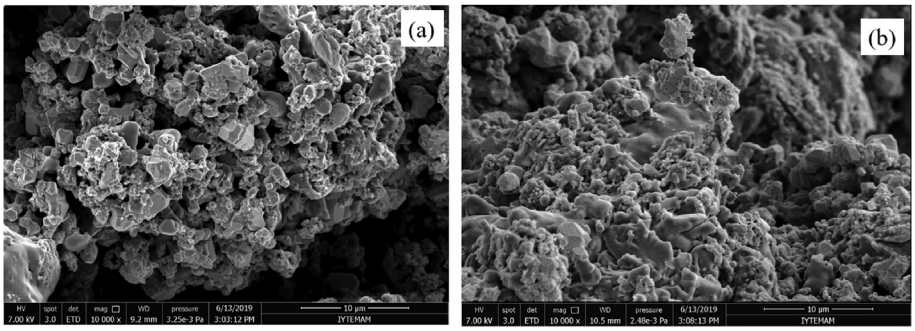

Fig. 5 – Surface morphologies of LSCF coating layers as deposited on GDC electrolyte. (a) Sample 4, and (b) Sample 5. Nozzle to substrate distance was 23 mm and 11 kV voltage was applied while the ceramic electrolyte specimen was heated at 400 °C.

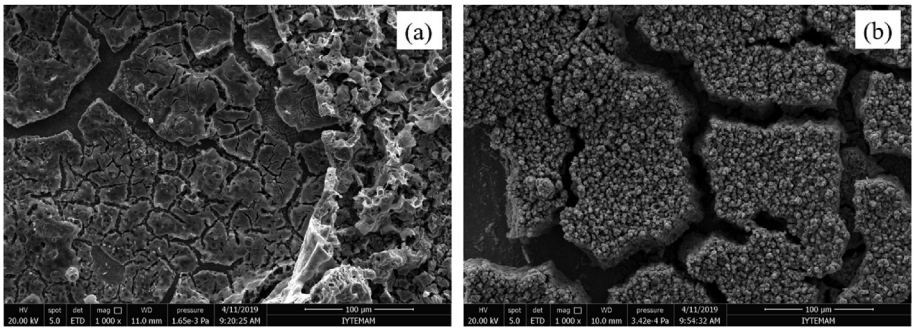

Fig. 6 – Surface morphologies of LSCF layers as deposited on GDC electrolyte. (a) Sample 6 and (b) sample 7.

manner and particles being overlapped. High voltage and large working distance lead to this macro-cracking due to almost complete solidification during the flight (Sample 7). This is also observed by other groups who observed that increasing the voltage and the working distance had the same kind of effects [15,54,55].

Evaporation of the new solvent couple is expected to be faster (boiling points of ethylene glycol and 2-butoxyethanol are 198 and 171 °C, respectively) [56] than conventional solvent couple (boiling points of ethanol and butyl carbitol are 78 and 230 °C, respectively). Hence, charged droplets are atomized faster since solution is decomposed faster. Evaporation of the solvent during flight occurs before landing on hot surface. For this reason, a powder-like agglomeration of tiny particles was observed in these samples except for Sample 4. Therefore, a more-detailed follow-up study of the investigation of ESD parameters is on-going.

Energy dispersive X-ray spectroscopy (EDX) analyses over the surface of coated samples were performed to track the variation of elemental concentration within the deposited layer. Different coating layer morphologies were obtained by varying the spraying parameters but using the same polymeric precursor solutions to yield the exact stoichiometries of $La_{0.6}Sr_{0.4}Co_{0.8}Fe_{0.2}O_{3-\delta}$ for all samples. Only two of them are reported here for the sake of brevity. Reported samples were prepared using exactly the same precursor solution. Fig. 7 indicates the changes in the elemental percentages in the deposited layer in two different samples. It is an evidence that the polymeric precursor solution is successful to achieve the formation of homogenous particles at nanoscale. Besides, although microstructure was changed, no significant compositional change was observed. Notice that, both samples were annealed at 700 °C after the deposition process was finished. Same kind of result is shown in other ESD studies in the literature [42]. Justification for the choice of these two samples lies in the fact that Sample 7 had large macrocracks and agglomerated areas which were quite dense. On the other hand, Sample 4 had a homogenously distributed layer with porous (coral) microstructure which is known in the literature to help reduce polarization resistance which leads to improved electrode performance [17,55].

The crystal structure of the deposited films was investigated by X-ray diffraction (XRD) from the surface (Fig. 8). LSCF and GDC phases were observed without any residual phases or chemical interaction phases between LSCF and GDC. LSCF peaks mostly overlapped with GDC peaks. Hence, distinct peaks corresponding to LSCF were observed at $2\theta = 22.5$ and 41° which are clearly seen in Fig. 8. These results also agreed well with the EDS results. For the sake of brevity, only one sample is reported (Sample 4) and other samples showed no significant difference compared with this one (i.e., no extra secondary peaks or residual-only intensity difference was observed). It is important to obtain exact stoichiometry due to the fact that $La_{1-x}Sr_xCo_{1-y}Fe_yO_{3-d}$ perovskite can easily change from orthorhombic to rhombohedral by simple slight change in X value [55–58]. Some groups which employed ethanol and

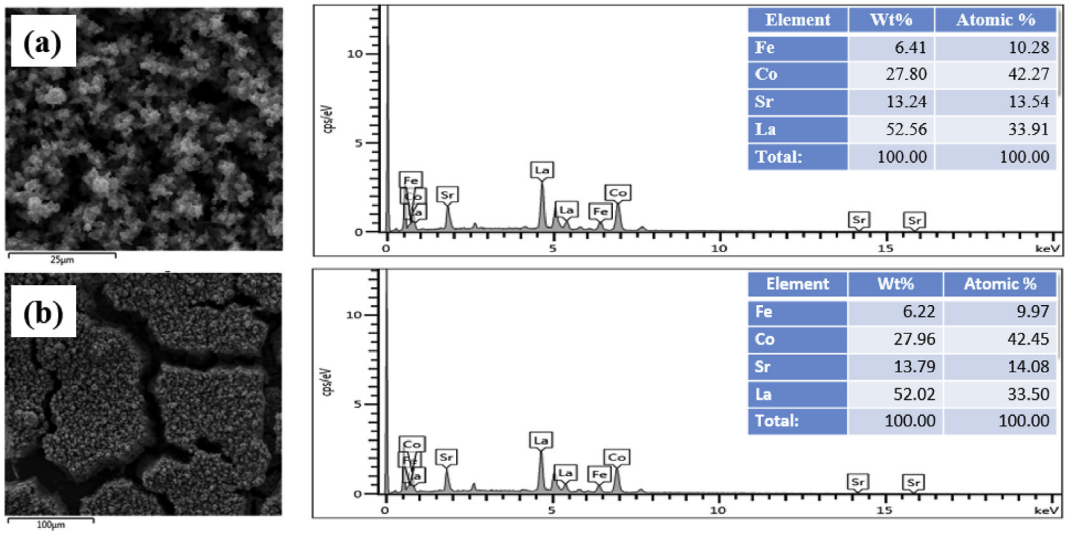

Fig. 7 – EDX analysis performed on samples with (a) coral (micro porous) surface coded "4" and (b) cracked (macro porous) surface of sample coded "7" (b). Elemental composition of electro-sprayed samples in atomic % and weight % were determined by semi-quantitative EDS analysis.

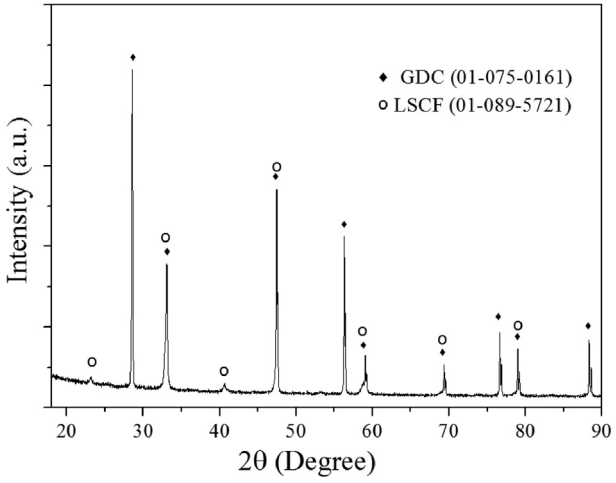

Fig. 8 – X-ray diffraction pattern of LSCF coated GDC symmetrical cell specimen (Sample 4). CuKα radiation was used in analysis. Peaks corresponding to LSCF and GDC phases are marked by ○ and ◆, respectively.

butyl carbitol solvent couple in precursor solution had observed some undesired peaks in addition to LSCF [31,59] while some others have not [42,60].

Two samples examined by EDX were chosen for electrochemical characterization tests due to their different microstructures. The Nyquist impedance plots of Samples 4 and 7 were measured at 700 °C in air, as shown in Fig. 9 (a). As explained above, these two samples were chosen to point out the effect of the type of coral microstructure with porous structure and dense textures (with macro cracks). The corresponding equivalent circuit model used for fitting measured data is also included in the figure as inset. A negligible error was present by using the equivalent circuits ($\chi 2 \sim 10^{-4}$). The intercept of the impedance response at high frequency presented ohmic resistance and represented with "Rs" in the equivalent circuit. This part was related with electrolyte resistance and the reason of the slight difference between the two samples was simply due to different thicknesses of the electrolyte layers which is also observed in other studies of the authors [51,52] as well as others [61,62]. Total polarization resistance was measured with the sum of R1 and R2 which was the size of impedance arc. However, as the coated samples were symmetrical, total polarization resistance was divided by two to find each resistance value of cathode (also denoted as area specific resistance or simply ASR). The results indicated that the microstructural modification via ESD technique successfully led to enhancement in electrochemical properties. Increasing the working distance, flow rate and applied voltage generated cracked films. Nearly more than two folds enhancement was obtained due to the coral structure of Sample 4. ASR values of Samples 4 and 7 were measured as 0.82 and 1.63 Ω cm^2, respectively. Porous nature of Sample 4 can be observed in Figs. 4b and 5a. This indicates that plenty of room is available for O_2 gas transport. Moreover, triple phase boundaries (TPBs) where cathode, electrode and gas phases meet are increased in coral microstructure. Eventually, ORR occurs over enlarged cathode surface and TPBs which bring about a decrease in polarization resistance. Therefore, reduced O_2 ions can be transported to GDC via TPBs and inside the bulk of LSCF [63]. Required steps and ORR mechanisms in porous structures are explained further in other studies of the authors [26]. Sample 7, on the other hand, had large cracks which isolated the pieces due to macroscopic porosities. Thus, active surface area and gas transport channels were compromised as manifested by the high-frequency semi-circle contribution [64]. This caused an increase in the polarization resistances.

Polarization resistance values (ASR) which were derived from impedance spectroscopy measurements of Samples 4 and 7 (measured at 500–700 °C with 50 °C intervals) are plotted against 1/T in Fig. 9 (b). Increasing some parameters led to degradation of film quality and macro cracks formed.

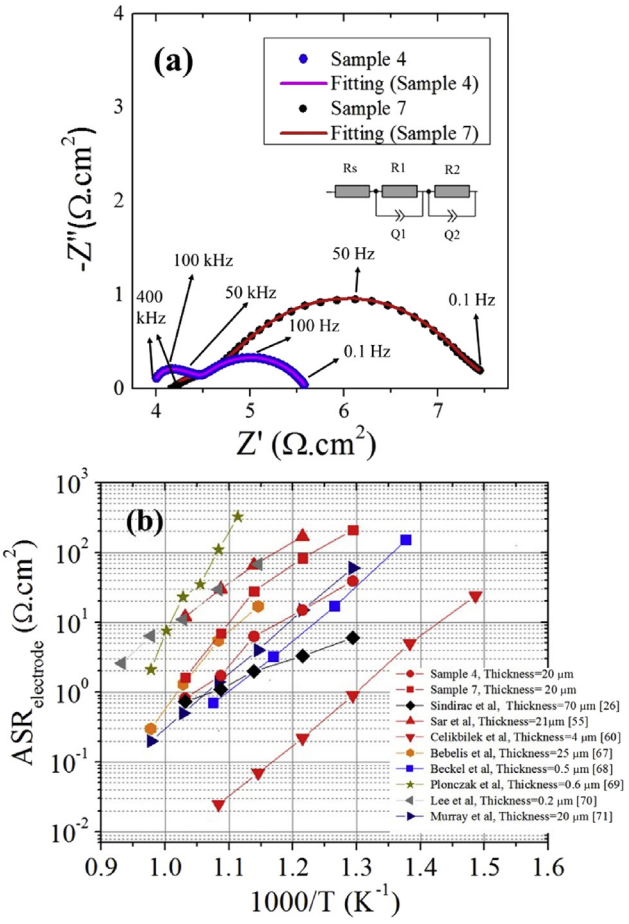

Fig. 9 – (a) Nyquist plots of EIS data for Sample 4 and 7 obtained at 700 °C. The equivalent circuit model used for fit is shown as inset. Obtained impedance data and summit frequencies are also included (b) Temperature dependence of ASR_{pol} ($ASR_{electrode}$) for the deposited films from Samples 4 and 7. The electrode polarization resistance data obtained by other methods are also included for comparison.

Therefore, area specific resistance of coral micro-structured sample was lower than the cracked sample in the temperature range of 500–700 °C. For a better comparison, studies involving conventionally formed LSCF methods like screen printing [67], infiltration [26], spray pyrolysis [68], PLD [69], RF magnetron sputtering [70], spin coating [71], with two different ESD study [55,60] are also added to that Fig. 9b. However, it is difficult to compare with the literature due to the different types of formation methods, annealing temperature and even thickness [42,65]. Yet, the lowest ever-measured ASR value in the literature of LSCF cathode was obtained [60] via ESD method. Also, the same group observed 80 times higher ASR value by using the same method [55,60,66]. Therefore, there is still significant room for development for this method to be investigated. While the ASR values measured here are acceptable, the ESD method with the new solvent couple proposed in this study needs to be improved further to find the optimum values.

Conclusions

Symmetrical LSCF electrode layers were successfully deposited on a previously fired (1400 °C) dense GDC electrolyte substrate by using polymeric precursor solution via low-cost ESD technique. Results have indicated that ethylene glycol and 2-butoxyethanol solvent couple may be used instead of ethanol-butyl carbitol solvent couple due to their capability to yield the exact stoichiometries without compromising the electrochemical properties. In this work, effects of main factors like the substrate temperature, applied voltage, flow rate, working distance and deposition duration on coating layer microstructure were studied. The results indicated that, a cone jet essential for providing a good coating, was successfully formed at the tip of the nozzle. In order to form a film via deposition, the substrate temperature must be over 350 °C for good adhesion. Changes in ESD parameters were found to have significant influence on the resulting morphology of the coated layer. EDX results showed that proper stoichiometric ratios of LSCF layer were kept after the spraying process. Besides, XRD results proved that no undesirable phase was formed during or after spraying. Impedance spectroscopy analysis indicated that the formation of coral structured film instead of cracked film caused a decrease in area specific resistance values. Encouraging results were observed in EIS measurements. These solvent couples need to be investigated more deeply in the future for optimization.

Acknowledgements

Authors would like to thank İYTE-MAM for their helps during analysis of the samples.

REFERENCES

[1] Sındıraç C, Akkurt S. Formation of $La_{1-x}Sr_xCo_{1-y}Fe_yO_{3-\delta}$ cathode materials from precursor salts by heating in contact with CGO electrolyte. Int J Hydrogen Energy 2016;41(40):18157–65.
[2] Da Silva FS, De Souza TM. Novel materials for solid oxide fuel cell technologies: a literature review. Int J Hydrogen Energy 2017;42:26020–36.
[3] Steele BCH. Material science and engineering: the enabling technology for the commercialisation of fuel cell systems. J Math Sci 2001;36(5):1053–68.
[4] Tarancón A. Strategies for lowering solid oxide fuel cells operating temperature. Energies 2009;2:1130–50.
[5] Liu M, Liu Y. Multilayer tape casting of large-scale anode-supported thin-film electrolyte solid oxide fuel cells. Int J Hydrogen Energy 2019;44(31):16976–82.
[6] Jung GB, Chang CT, Yeh CC, Nguyen XV, Chan CH, Lin CY, Yu JW, Lee WT, Chang SW, Kao IC. Study of reversible solid oxide fuel cell with different oxygen electrode materials. Int J Hydrogen Energy 2016;41(16):21802–11.
[7] Al Zahrani A, Dincer I, Li X. A performance assessment study on solid oxide fuel cells for reduced operating temperatures. Int J Hydrogen Energy 2015;40(24):7791–7.
[8] Shu L, Sunarso J, Hashim SS, Mao J, Zhou W, Liang F. Advanced perovskite anodes for solid oxide fuel cells: a review. Int J Hydrogen Energy 2019;44(59):31275–304.

[9] Jiang SP. Development of lanthanum strontium cobalt ferrite perovskite electrodes of solid oxide fuel cells- A review. Int J Hydrogen Energy 2019;44(14):7448–93.

[10] Liu M, Ding D, Blinn K, Li X, Nie L, Liu M. Enhanced performance of LSCF cathode through surface modification. Int J Hydrogen Energy 2012;37:8613–20.

[11] Ai N, Chen KF, Jiang SP. A La0.8Sr0.2MnO3/La0.6Sr0.4Co0.2Fe0.8O3-delta core-shell structured cathode by a rapid sintering process for solid oxide fuel cells. Int J Hydrogen Energy 2017;42:7246–51.

[12] Sun LP, Rieu M, Viricelle JP, Pijolat C, Zhao H. Fabrication and characterization of anode-supported single chamber solid oxide fuel cell based on La0.6Sr0.4Co0.2Fe0.8O3–δ–Ce0.9Gd0.1O1.95 composite cathode. Int J Hydrogen Energy 2014;39(2):1014–22.

[13] DiGiuseppe G, Sun L. Electrochemical performance of a solid oxide fuel cell with an LSCF cathode under different oxygen concentrations. Int J Hydrogen Energy 2011;36(8):5076–87.

[14] Fuentes RO, Baker RT. Synthesis and properties of Gadolinium-doped ceria solid solutions for IT-SOFC electrolytes. Int J Hydrogen Energy 2008;33(13):3480–4.

[15] Marinha D, Rossignol C, Djurado E. Influence of electrospraying Parameters on the microstructure of La0.6Sr0.4Co0.2Fe0.8O3-d films for SOFCs. J Solid State Chem 2009;182:1742–8.

[16] Beckel D, Bieberle-Hütter A, Harvey A, Infortuna A, Muecke UP, Prestat M, Rupp JLM, Gauckler JL. Thin films for micro solid oxide fuel cells. J Power Sources 2007;173(1):325–45.

[17] Marinha D, Dessemond L, Djurado E. Comprehensive review of current developments in IT-SOFCs. Curr Inorg Chem 2013;3:2–22.

[18] Mah JCW, Muchtar A, Somalu MR, Ghazali MJ. Metallic interconnects for solid oxide fuel cell: a review on protective coating and deposition techniques. Int J Hydrogen Energy 2017;42:9219–29.

[19] Vandieten VEJ, Schoonman J. Thin-film techniques for solid oxide fuel-cells. Solid State Ionics 1992;57(1–2):141.

[20] Takeyama T, Takahashi N, Nakamura T, Itoh S. Delta-Bi_2O_3 thin films deposited on dense YSZ substrates by CVD method under atmospheric pressure for intermediate temperature SOFC applications. Surf Coating Technol 2006;200(16–17):4797–801.

[21] Liu Y, Rauch W, Zha SW, Liu ML. Fabrication of Sm0.5SrO.5CoO0.3-δ -Sm0.lCeO0.9O2-δ cathodes ta for solid oxide fuel cells using combustion CVD. Solid State Ionics 2004;166(3–4):261–8.

[22] Rezugina E, Thomann AL, Hidalgo H, Brault P, Dolique V, Tessier Y. Ni- YSZ films deposited by reactive magnetron sputtering for SOFC applications. Surf Coating Technol 2010;204(15):2376–80.

[23] Otani M, Tsukui S, Yoshida K, Umezaki Y, Mukai T. Fabrication of Gd0.5Sr0.5C003 film for SOFC cathode by pulsed laser deposition. Solid State Ionics 2010;180(40):1667–71.

[24] Heiroth S, Lippert Th, Wokaun A, Döbeli M. Microstructure and electrical conductivity of YSZ thin films prepared by pulsed laser deposition. Appl Phys Mater Sci Process 2008;93(3):639–43.

[25] Joo JH, Choi GM. Electrical conductivity of YSZ film grown by pulsed laser deposition. Solid State Ionics 2006;177(11–12):1053–7.

[26] Sındıraç C, Buyukaksoy A, Akkurt S. Electrochemical performance of La0.6Sr0.4Co0.2Fe0.8O3–Ce0.9Gd0.1O2-δ composite SOFC cathodes fabricated by electrocatalyst and/or electrocatalyst-ionic conductor infiltration. J Sol Gel Sci Technol 2019;92(1):45–56.

[27] Tsai MJ, Chu CL, Lee S. La0.6Sr0.4Co0.2Fe0.8O3-δ coatings for solid oxide fuel cell interconnect deposited by screen printing. J Alloys Compd 2010;489(2):576–81.

[28] Chen M, Kim BH, Xu Q, Ahn BG, Huang DP. Fabrication and performance of anode-supported solid oxide fuel cells via slurry spin coating. J Membr Sci 2010;360(1–2):461–8.

[29] Jiang SP. Nanoscale and nano-structured electrodes of solid oxide fuel cells by infiltration: advances and challenges. Int J Hydrogen Energy 2012;37:449–70.

[30] Princivalle A, Djurado E. Nanostructured LSM/YSZ composite cathodes for IT-SOFC: a comprehensive microstructural study by electrostatic spray deposition. Solid State Ionics 2008;179:1921–8.

[31] Taniguchi I, Schoonman J. Electrostatic spray deposition of perovskite-type oxides thin films with porous microstructure. J Mater Synth Process 2003;10(5):267–75.

[32] Taniguchi I, van Landschoot RC, Schoonman J. Fabrication of $La_{1-x}Sr_xCo_{1-y}Fe_yO_3$ thin films by electrostatic spray deposition. Solid State Ionics 2003;156:1–13.

[33] Chen CH, Kelder EM, Jak MJG, Schoonman J. Electrostatic spray deposition of thin layers of cathode materials for lithium battery. Solid State Ionics 1996;86–88:1301–6.

[34] Chen CH, Kelder EM, van der Put PJM, Schoonman J. Morphology control of thin LiCoO2 films fabricated using the electrostatic spray deposition (ESD) technique. J Mater Chem 1996;6(5):765–71.

[35] Jaworek A, Sobczyk AT, Krupa A. Electrospray application to powder production and surface coating. J Aerosol Sci 2018;125:57–92.

[36] Jaworek A. Electrospray droplet sources for thin film deposition. J Mater Sci 2007;42:266–97.

[37] Castillo JL, Martin S, Rodriguez-Perez D, Higuera FJ, Garcia-Ybarra PL. Nanostructured Porous coatings via electrospray atomization and deposition of nanoparticle suspensions. J Aerosol Sci 2018;125:148–63.

[38] Yadav JB, Park JW, Jung KD, Joo OS. Low Pt loading, wide area electrospray deposition technique for highly efficient hydrogen evolving electrode in photoelectrochemical cell. Int J Hydrogen Energy 2010;35:6541–8.

[39] Ubeda D, Canizares P, Ferreira-Aparicio P, Chaparro AM, Lobato J, Rodrigo MA. Life test of a high temperature PEM fuel cell prepared by electrospray. Int J Hydrogen Energy 2016;41:20294–304.

[40] Nguyen T, Djurado E. Deposition and characterization of nanocrystalline tetragonal zirconia films using electrostatic spray deposition. Solid State Ionics 2001;138:191–7.

[41] He Q, Selman JR, Nash P. Continuous fabrication of SOFC assembly by ESD technique- dense thin film YSZ electrolyte. ECS Trans 2014;58(45):89–99.

[42] Marinha D, Dessemond L, Djurado E. Microstructure-electrical properties of original LSCF films deposited by ESD for IT-SOFCs. ECS Trans 2010;28(11):93–103.

[43] Kudoh Y, Saito S, Takahashi T. Application of an electro spray deposition (ESD) method to control the pre-tilt angle in a nematic LC cell. Mol Cryst Liq Cryst 2011;546:156–62.

[44] Rietveld IB, Kobayashi K, Yamada H, Matsushige K. Electrospray deposition, model, and experiment: toward general control of film morphology. J Phys Chem B 2006;110:23351–64.

[45] Chen CH, Buysman AAJ, Kelder EM, Schoonman J. Fabrication of LiCoO2 thin film cathodes for rechargeable lithium battery by electrostatic spray pyrolysis. Solid State Ionics 1995;80:1–4.

[46] Jaworek A, Sobczyk AT. Electrospraying route to nanotechnology: an overview. J Electrost 2008;66:197–219.

[47] Princivalle A. Nouvelle électrode à gradients pour piles à combustible à oxyde électrolyte solide. Grenoble INP: Ph.D. Thesis; 2006.

[48] Bailly N, Georges S, Djurado E. Electrical properties od electrospray YSZ thin films for intermediate temperature solid oxide fuel cells (IT-SOFC). ECS Trans 2012;45(1):413–20.
[49] Taniguchi I, Hosokawa T. Deposition of SDC and Nio-SDC thin films and their surface morphology control by electrostatic spray deposition. J Alloys Compd 2008;460:464–71.
[50] Sındıraç C, Cakirlar S, Buyukaksoy A, Akkurt S. Lowering the sintering temperature of solid oxide fuel cell electrolytes by infiltration. J Eur Ceram Soc 2019;39(2–3):409–17.
[51] Sındıraç C, Buyukaksoy A, Akkurt S. Electrical properties of gadolinia doped ceria electrolytes fabricated by infiltration aided sintering. Solid State Ionics 2019;340:115020.
[52] Sındıraç C, Ahsen A, Ozturk O, Akkurt S, Birss VI, Buyukaksoy A. Fabrication of LSCF and LSCF-GDC nanocomposite thin films using polymeric precursors. Ionics 2020;26:913–25.
[53] Neagu R, Perednis D, Princivalle A, Djurado E. Initial stage in zirconia coatings using ESD. Chem Mater 2005;17(4):902–10.
[54] Neagu R, Perednis D, Princivalle A, Djurado E. Influence of the process parameters on the ESD synthesis of thin film YSZ electrolytes. Solid State Ionics 2006;177:1981–4.
[55] Sar J, Charlot F, Almedia A, Dessemond L, Djurado E. Coral microstructure of graded CGO/LSCF oxygen electrode by electrostatic spray deposition for energy (IT-SOFC, SOEC). Fuel Cell 2014;14(3):357–63.
[56] Ksapabutt B, Chalermkiti T, Wongkasemjit S, Panapoy M. Fabrication of scandium stabilized zirconia thin film by electrostatic spray deposition technique for solid oxide fuel cell electrolyte. Thin Solid Films 2010;518:6518–21.
[57] Prado F, Grunbaum N, Caneiro A, Manthiram A. Effect of La3+ doping on the perovskite-to-brownmillerite transformation in Sr1−xLaxCo0.8Fe0.2O3−δ (0≤x≤0.4). Solid State Ionics 2004;167:147.
[58] Gu YJ, Yang ZN, Chen YB, Liu HQ, Wu HK, Chen L, Wang M, Zuo LL, Huang XW, Liu XB, Wei WG, Lu C, Hu Y, Guo Z, Hu ZW. Structural analysis of multiphase La1-XSrxCo1-XFexO3-δ. Adv Mater Res 2011;177:74–7.
[59] Kwon HT, Kim J. Synthesis and characterization of porous La1-xSrxCo1-yFeyO3-d membranes fabricated using by electrostatic spray deposition. J Kor Phys Soc 2009;54(3):1223–7.
[60] Celikbilek O, Jauffres D, Siebert E, Dessemond L, Burriel M, Martin CL, Djurado E. Rational design of hierarchically nanostructured electrodes for solid oxide fuel cells. J Power Sources 2016;333:72–82.
[61] Prakash BS, Kumar SS, Aruna ST. Effect of composition on the polarization and ohmic resistances of LSM/YSZ composite cathodes in solid oxide fuel cell. Bull Mater Sci 2017;40(3):441–52.
[62] Hilal N, Ismail AF, Wright C. Membrane fabrication. CRC Press page; 2015. p. 375.
[63] Adler SSB. Factors governing oxygen reduction in solid oxide fuel cell cathodes. Chem Rev 2004;104(1):4791.
[64] Tomov RI, Mitchell-Williams T, Gao C, Kumar RV, Glowacki BA. Performance optimization of LSCF/Gd:CeO2 composite cathodes via single-step inkjet printing infiltration. J Appl Electrochem 2017;47:641–51.
[65] Leng Y, Chan SH, Liu Q. Development of LSCF-GDC composite cathodes for low-temperature solid oxide fuel cells with thin film GDC electrolyte. Int J Hydrogen Energy 2008;33:3808–17.
[66] Marinha D, Dessemond L, Cronin JS, Wilson JR, Barnett SA, Djurado E. Microstructural 3D reconstruction and performance evaluation of LSCF cathodes obtained by electrostatic spray deposition. Chem Mater 2011;23:5340.
[67] Bebelis S, Kotsionopoulos N, Mai A, Tietz F. Electrochemical characterization of perovskite-based SOFC cathodes. J Appl Electrochem 2006;37:15–20.
[68] Beckel D, Muecke U, Gyger T, Florey G, Infortuna A, Gauckler L. Electrochemical performance of LSCF based thin film cathodes prepared by spray pyrolysis. Solid State Ionics 2007;178:407–15.
[69] Plonczak P, Søgaard M, Bieberle-Hütter A, Hendriksen PV, Gauckler LJ. Electrochemical characterization of La0.58Sr0.4Co0.2Fe0.8O3−δ thin films electrodes prepared by pulsed laser deposition. J Electrochem Soc 2012;159:B471.
[70] Lee JW, Liu Z, Yang L, Abernathy H, Choi SH, Kim H-E, Liu M. Preparation of dense and uniform La0.6Sr0.4Co0.2Fe0.8O3−δ (LSCF) films for fundamental studies of SOFC cathodes. J Power Sources 2009;190:307–10.
[71] Murray EP, Sever MJ, Barnett SA. Electrochemical performance of (La,Sr)(Co,Fe)O3−(Ce,Gd)O2 composite cathodes. Solid State Ionics 2002;148:27–34.